DESCENDING THERMAL SHOCK TESTS ON A HIGH-ALUMINA REFRACTORY BRICK: EXPERIMENTAL EVALUATION AND MODELLING APPROACH

Jean-François Trelcat, Sandra Abdelouhab
BCRC-INISMa, Belgian Ceramic Research Centre, Mons, Belgium

Erwan Brochen, Christian Dannert
Forschungsgemeinschaft Feuerfest e.V., Höhr-Grenzhausen, Germany

ABSTRACT
Thermal shock tests have been performed on a high-alumina refractory brick according to the EN 993-11 standard. Numerical modelling with Cohesive Element Method involving the insertion of embedding zero-thickness cohesive elements can predict with a relatively good accuracy the cracking phenomenon in thermally shocked refractory materials. The identification of the cohesive elements' parameters, i.e. the tensile strength σ_{max}, the fracture energy G_{IC} and the stiffness K, can be easily obtained by the means of both experiments and simulations of wedge splitting tests. A possible correlation between meshing size and microstructure was highlighted.

INTRODUCTION
To evaluate the thermal shock resistance of a refractory material, samples with a well-defined geometry are subjected to specific test conditions, in accordance with the specifications of standardised methods. Among the most widely used standards, the ISO 21736:2018, EN 993-11, and ASTM-C-1171 standards can be cited. All of these standardised procedures describe quench cycles (or descending thermal shock) between 950 °C (ISO and EN) or 1200 °C (ASTM) and ambient temperature, in water (ISO) or compressed air (EN and ASTM).
The numerical modelling of these thermal shocks allows to complement and deepen the standardised experimental tests by offering the possibility to predict the behaviour of refractory materials subjected to severe thermal loads. In this regard, the Cohesive Element Method (CEM) has proven its effectiveness in analysing structural cracking and crack propagation compared to other discontinuous methods. By integrating zero-thickness cohesive elements between body elements, CEM can model the entire crack evolution process and enable their bifurcation, which requires the identification of numerous parameters generally estimated using experimental, trial-and-error or empirical methodologies.
This study focuses on a simple method for identifying these parameters and the correlation between simulations and experimental thermal shock tests. The thermal shock tests were investigated according to the EN 993-11 standard on a high-alumina refractory brick with a content of Al_2O_3 above 99% and ceramic bonded. The thermo-mechanical simulations were performed with the Abaqus software.

MATERIAL PARAMETERS IDENTIFICATION BY WEDGE SPLITTING TESTS SIMULATIONS
As illustrated in figure 1, the stress evolution of cohesive elements can be described by the traction-separation criterion, which consists of a linear elastic stage followed by a damage initiation and evolution process.

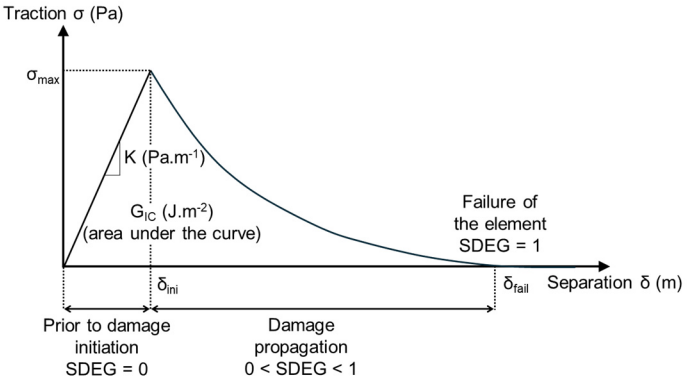

Fig. 1: Parameters of the traction-separation law.

The damage initiation is governed by two parameters, the initial stiffness K and the tensile strength σ_{max}. During the damage evolution, the (δ,σ) curve is a function of the fracture energy G_{IC}, corresponding to the area under the curve, and the softening behaviour. In this work, an exponential softening behaviour was employed to characterise the degradation stage. In Abaqus, the damage variable is denoted as SDEG with SDEG = 0 for $\delta \leq \delta_{ini}$, 0 < SDEG < 1 for $\delta_{ini} < \delta < \delta_{fail}$, and SDEG = 1 at the δ_{fail} element failure.
In this study, the three previous parameters, K, σ_{max} and G_{IC}, were identified in relation to temperature by the mean of wedge splitting tests (WST) and the associated numerical simulations. According to the works of Brochen *et al.* [1], WST were performed at 20 °C and 1000 °C on cubic test pieces (100 × 100 × 75 mm^3) machined from a high-alumina refractory brick. A groove, used to position and accommodate the load transmission system in order to transfer the horizontal splitting forces to the ligament area, was cut into the cubic sample with a width of 24 mm and a depth of 22 mm. Additionally, a starter notch of 3 mm × 12 mm and two lateral crack-guiding notches of 3 mm × 6 mm were also sawed in the test pieces. The alumina load transmission plates, used to convert the vertical force applied on the top of the wedge into a horizontal splitting force, has an angle of 10°, a height of 24 mm, a length of 75 mm and a thickness of 7 mm. To ensure sufficient stability, the test specimens were centered on a rectangular bar acting as a linear bearing with a height of 7 mm, a thickness of 7 mm and a length of 75 mm. A constant displacement-controlled loading rate of 0,5 mm/min was applied throughout the duration of the test. The horizontal force F and the opening of the test piece δ (crack mouth opening displacement) were monitored and compiled in a load-displacement diagram.
For each investigated temperature, the experimental tensile strengths σ_{max} were estimated by dividing the maximum load reached during the test with the loaded groove surface (approximated to 75 × 22 mm^2). These experimental data (table 1) were used directly and no additional identification was considered necessary.
The experimental specific fracture energies G_{IC} were calculated from the area below the load-displacement curve and the ligament area according to:

$$G_{IC} = \frac{1}{A}\int_0^{\delta_f} F_H d\delta_H \quad (1)$$

where F_H is the horizontal load, A the fracture area, δ_H the measured horizontal displacement and δ_f the horizontal displacement at 15% of the maximum load.

According to temperature, the stiffness K and the specific fracture energy G_{IC} parameters were adjusted by means of 2D space numerical simulations of the experimental wedge splitting test. The procedure consisted of meshing the WST sample with 4-nodes CPE4T solid elements and replacing their edges with 4-nodes COH2D4T zero-thickness cohesive elements (the insertion methodology based on the works of Li *et al.* [2] is not described here). Four meshing sizes were investigated: 1, 2, 3 and 4 mm. The contact condition between the alumina load transmission plates and the sample was defined without separation and a friction coefficient of 0,3. For the bottom contact, the same friction coefficient of 0,3 was applied but the separation was allowed to avoid the appearance of an aberrant counterforce. A total displacement equal to the experimental one was applied on the left and right load transmission plates. By fixing the Young's modulus E, the Poisson's ratio ν and the tensile strength σ_{max} in respect to the investigated temperature, the procedure consisted of testing different sets of (K, G_{IC}) values to find the ones fitting with the more accuracy the experimental data. It should be noted that the Impulse Excitation Technique (IET) was used to estimate the hot Young's modulus (from ambient to 1200 °C) and the Poisson's ratio (at room temperature) on a high-alumina refractory brick beam of 15 × 25 × 120 mm^3. Some values of the hot Young's modulus and the Poisson's ratio are presented in table 2.

Figure 2 shows the as-obtained numerical load-displacement curves at 20 °C and 1000 °C and for each investigated meshing sizes. To appreciate the quality of the curve fitting, the experimental data are also indicated by black triangles.

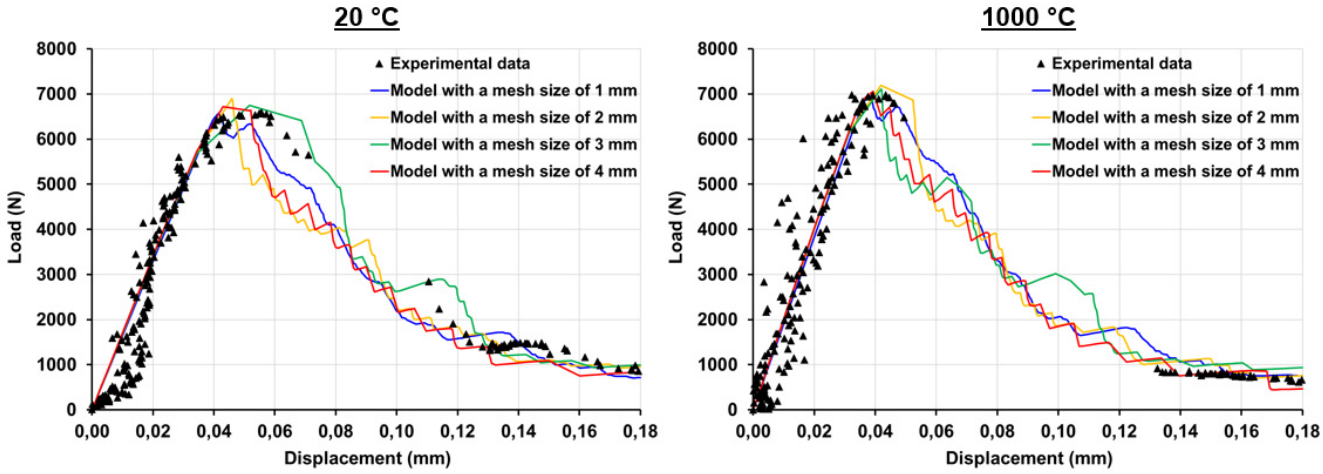

Fig. 2: Experimental data and numerical load-displacement curves obtained at 20 °C and 1000 °C.

Independently of the used meshing sizes, the numerical curves fit with a relatively good accuracy the experimental data. The stiffnesses identified by this procedure faithfully reproduce the elastic part of the curve. Table 1 summarises the as-obtained numerical stiffnesses and two specific fracture energies, the input value and the calculated value according to (1). For comparative purposes, experimental G_{IC} data are also presented.

Tab. 1: Experimental data and input cohesive elements' parameters obtained for each investigated meshing sizes at 20 °C and 1000 °C.

	20 °C					1000 °C				
	Simulation				Experiment	Simulation				Experiment
Meshing size (mm)	1	2	3	4	-	1	2	3	4	-
σ_{max} (MPa)	4,03	4,03	4,03	4,03	4,03	4,17	4,17	4,17	4,17	4,17
K (GPa.m^{-1})	11000	5200	3700	2900	-	13000	6300	4500	3500	-
Input G_{IC} (J.m^{-2})	140	165	165	175	-	135	150	150	165	-
Calculated G_{IC} (J.m^{-2})	103	101	110	103	109	97	96	94	91	94

For each investigated temperature, the stiffness parameter K decreases with increasing meshing sizes. In the same way, the input G_{IC} rises with larger meshing sizes. These trends can be attributed to the fact that as the meshing becomes less dense, the number of cohesive elements decreases. As a result, the model's stiffness becomes more elastic, which accounts for the reduced stiffness parameter needed to match the elastic part of the experimental curve. Additionally, the G_{IC} input parameter must be increased to offset the lower cohesion and prevent the maximum load F from being too low in comparison to the experimental curves. Overall, regardless of the meshing sizes used, it's important to note that the G_{IC} input values must be significantly higher than the experimental ones to achieve a strong correlation between the experimental and numerically calculated specific fracture energies.

THERMAL SHOCK SIMULATIONS

Experimental procedure

The standard EN 993-11 consists of cooling a refractory product using a compressed air jet. The sample is first preheated to 300 °C overnight and then placed in a furnace at 950 °C for 45 minutes. At the exit of the furnace, the sample is placed at the center of a steel plate of 400 × 250 × 20 mm^3 and then cooled for 5 minutes with an air pressure of 0,1 MPa. The 8 mm in diameter nozzle used for the cooling process is positioned at a height of 100 mm above the middle of the top surface of the specimen.

In this work, three high-alumina refractory brick's beams of 25 × 25 × 150 mm^3 were thermally shocked in the previous conditions. The dynamic Young's modulus was measured by IET before and after the thermal shock test.

Coupled temperature-displacement simulations of the thermal shock

The beam of the high-alumina refractory brick was modeled in both 2D and 3D spaces with the same meshing procedure and sizes used in the WST simulations. In 2D space, the dimensions were 25 mm × 150 mm, using 4-node CPE4T solid elements and 4-node COH2D4T zero-thickness cohesive elements. In 3D space, the dimensions were 25 mm × 25 mm × 150 mm, employing 8-node C3D8T solid elements and 8-node COH3D8T zero-thickness cohesive elements. Depending on the used meshing size, the cohesive elements' input parameters were the same ones presented in table 1. In addition to the previous parameters and to perform the thermo-mechanical simulations, table 2 details the density ρ, the expansion coefficient α, the specific heat Cp, the thermal conductivity λ, the Young's modulus and the Poisson ratio's of the high-alumina refractory brick.

Tab. 2: Input data of the high-alumina refractory brick.

Temperature (°C)	ρ (kg.m^{-3})	$\alpha_{ref.293K}$ (K^{-1})	Cp (J.Kg^{-1}.K^{-1})	λ (W.m^{-1}.K^{-1})	E (GPa)	ν
20			-	-	116	
400			970	3,6	109	
600	3350	8,67 × 10^{-6}	1020	3,3	91	0,146
800			1060	3,1	100	
1000			1100	3,1	113	

The cohesive elements are not used as a heat source but rather serve as a pathway for heat transfer between the solid elements. To ensure accurate and efficient heat transfer, a cohesive elements' gap conductance of 10^9 W.m^{-2}.K^{-1} was chosen [3]. According to the thermal shock test conditions, the initial temperature of the high-alumina refractory brick's beam was fixed at 300 °C. A first transient coupled temperature-displacement step was used to simulate the loading of the beam inside the furnace. To reach a temperature of 950 °C, a convective heat transfer coefficient of 10 W.m^{-2}.K^{-1} and an emissivity of 0,9 were applied on each external edges/faces of the beam. The natural cooling induced by the air convection at the exit of the furnace was performed by a second transient coupled temperature-displacement step. The time period was evaluated at 15 seconds. On each external edges/faces of the beam, a convective heat transfer coefficient of 12 W.m^{-2}.K^{-1} and an emissivity of 0,8 (based on the data proposed by Routschka *et al.* [4]) were applied. The final step, modelling the 300 seconds time period of the thermal shock itself, should consider the cooling due to the use of a compressed air jet. To define the convective heat transfer coefficients to be applied to the top edge/face of the beam, the impinging jet model of Tawfek *et al.* [5] was used. Without going into detail, the average convective heat transfer coefficient decreases exponentially from 883 W.m^{-2}.K^{-1} at the center of the beam to 468 W.m^{-2}.K^{-1} at the edges of the beam. The bottom thermal contact interaction between the steel plate and the beam was modelled with a contact conductance of 125 W.m^{-2}.K^{-1}. This coefficient was calculated following a series model by considering the thermal conductivity and the thickness of each material (for the steel plate, λ = 50 W.m^{-1}.K^{-1}). The bottom contact emissivity was defined as a function of an effective view factor between the two surfaces and was assumed to be equal to 0,8. For the other edges/faces, a natural convective heat transfer coefficient of 12 W.m^{-2}.K^{-1} and an emissivity of 0,8 were applied.

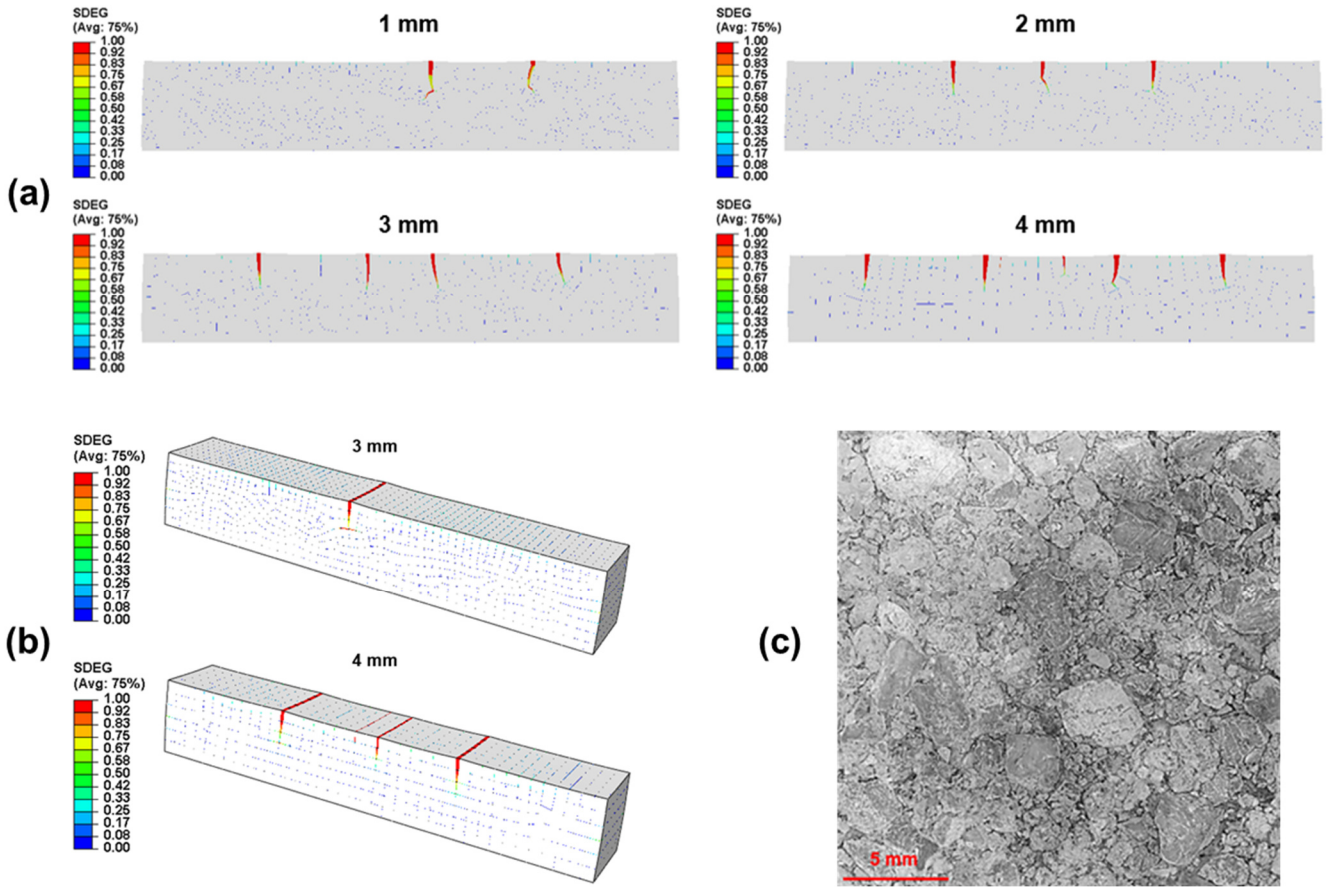

Fig. 3: Thermal shock simulations according to the investigated meshing sizes: final state of the SDEG variable. (a) 2D space. (b) 3D space. (c) Microstructure of the high-alumina refractory brick.

Figure 3a shows the final state of the SDEG variable obtained for 2D space thermal shock simulations with a meshing size of 1, 2, 3 and 4 mm. The variation in meshing size has a notable impact on the number of the cracks. From the figure, it can be observed that as the mesh edge length decreases, the preset crack paths become denser. This indicates that the evolution path of the crack becomes progressively more complex, with a greater likelihood of bifurcation. The development trend of the cracks in the figure reveals that as the mesh becomes finer, the number of the cracks decreases (5 with a meshing size of 4 mm to 2 with a meshing size of 1 mm). In the same way, the crack tortuosity increases with decreasing meshing sizes. The validation of these simulations in regard to experiment is presented in the next section.
To verify a possible correlation between meshing size and microstructure (the assembly of solid elements would thus play the role of aggregates, while the cohesive elements would form the bonding phase), two additional 3D space simulations (figure 3b) were performed according to the microstructure of the high-alumina refractory brick (figure 3c). The chosen meshing sizes of 3 and 4 mm were in accordance with the coarser grain size of the microstructure. As previously, the number of the cracks increases with increasing meshing sizes (4 with a meshing size of 4 mm to 1 with a meshing size of 3 mm). Nevertheless, and comparing to the equivalent 2D space simulations, the number of the cracks decreases from 4 to 1 for a meshing size of 3 mm and from 5 to 4 for a meshing size of 4 mm. The difference can be easily attributed to triaxial effects and/or some variation between 2D and 3D heat transfer approximations.

Validation of the thermal shock simulations
The validation of thermal shock simulations in regard to experiments was performed by the means of frequency analyses. The results are presented in table 3. The experimental frequencies measured by IET before the thermal shock were compared to the numerical ones obtained from both 2D and 3D space classical models without crack and an arbitrary chosen meshing size of 1 mm (table 3 in blue). In the same way, and to verify the accuracy of the cracked models in comparison to experimental data, numerical flexural frequencies (2D space) and both numerical flexural/torsional frequencies (3D space) were obtained by performing simulations at each investigated meshing sizes and by considering the experimental value of the dynamic Young's modulus measured before the thermal shock (table 3 in red).

Tab. 3: Flexural frequencies - comparison between experiment and simulation (the percentages correspond to the ratio of experimental and numerical values).

	Experiment		Simulation with a meshing size of				
	Before shock	After shock	Before shock	After shock			
			1 mm	1 mm	2 mm	3 mm	4 mm
2D space							
Flexion (Hz)	6058	5020	6076 (99%)	4321 (86%)	4491 (89%)	4450 (89%)	4754 (95%)
3D space							
Flexion (Hz)	6058	5020	6016 (99%)	-	-	4734 (94%)	4821 (96%)
Torsion (Hz)	11663	10050	11579 (99%)	-	-	10692 (94%)	10739 (93%)

Regardless of the space used, the flexural and torsional frequency values obtained with the non-cracked model correspond well to the experimental data. For the cracked 2D models, the best fit for the flexural frequency is obtained with a mesh size of 4 mm (4754 Hz vs. 5020 Hz). This observation is confirmed in 3D space (4821 Hz vs. 5020 Hz). More generally, and independently of the used meshing size, both flexural and torsional frequencies obtained with the 3D modelling are consistent with the experimental data. These results suggest a plausible correlation between mesh size and microstructure. Thus, the technique of inserting cohesive elements into finite element analysis seems to deviate from traditional continuum mechanics. Nevertheless, further work is needed to confirm these hypotheses.

CONCLUSION AND OUTLOOKS
Numerical modelling with Cohesive Element Method involving the insertion of embedding zero-thickness cohesive elements can predict with a relatively good accuracy the cracking phenomenon in thermally shocked refractory materials. Based on the present work, some conclusions can be proposed:
1. The identification of the cohesive elements' parameters, i.e. the tensile strength σ_{max}, the fracture energy G_{IC} and the stiffness K, can be easily obtained by the means of both experiments and simulations of wedge splitting tests.
2. A possible correlation between meshing size and microstructure was highlighted.

Nevertheless, further works are needed:
1. Test the method on other refractory materials and/or under other conditions (i.e. ascending thermal shock).
2. Investigate further the hypothesis of a correlation « meshing size/microstruture ».

ACKNOWLEDGEMENTS
The author acknowledges the NBN and SPF Economy for their financial support of this study conducted within the framework of the CHOTHERM project, grant agreement PN22A56.

REFERENCES
[1] Erwan Brochen, Christian Dannert, Juliane Paul, Olaf Krause. Investigation of fracture behavior of typical refractory materials up to service temperatures. International Journal of Ceramic Engineering & Science, 2022, p. 1-9
[2] Li, S., Chen, Z., Li, W. et al. An FE Simulation of the Fracture Characteristics of Blunt Rock Indenter Under Static and Harmonic Dynamic Loadings Using Cohesive Elements. Rock Mechanics and Rock Engineering 56, 2023, p. 2935-2947
[3] Jian Ding, Xin Wang, Mengke Lei, Kaidi Jiang, Zhishen Wu. Cohesive element-based chemo-thermo-mechanical multi-field coupled cracking simulation of early-age concrete. Theoretical and Applied Fracture Mechanics 130 (104296), 2024
[4] Gerald Routschka et al. Handbook of Refractory Materials - Design, Properties, Testings. 4th Edition, Vulkan, 2012
[5] A. A. Tawfek. Heat transfer and pressure distributions of an impinging jet on a flat surface. Heat and Mass Transfer 32, 1996, p. 49-54